Colloid Polym Sci 277:607–626 (1999)

ORIGINAL CONTRIBUTION

K. Tauer
R. Deckwer
I. Kühn
C. Schellenberg

A comprehensive experimental study of surfactant-free emulsion polymerization of styrene

Received: 25 November 1998
Accepted in revised form: 25 January 1999

K. Tauer (✉) · R. Deckwer
C. Schellenberg
Max-Planck-Institut für Kolloid- und Grenzflächenforschung
Kantstrasse 55
D-14513 Teltow-Seehof, Germany
e-mail: ktau@mpikg-teltow.mpg.de
Tel.: +49-3328-46258
Fax: +49-3328-46255

I. Kühn
BASF AG, D-67056 Ludwigshafen
Germany

Abstract Comprehensive experimental results are presented for surfactant-free emulsion polymerization of styrene with water-soluble, ionic initiators. Special emphasis is placed on the particle nucleation, the chemical structure of the nucleating species, the change of latex, particle and polymer properties as well as the development of particle morphology with polymerization time. Under special conditions the appearance in transmission electron microscopy pictures of less electron dense anomalous particles is observed. The formation of these structures is discussed and possible formation mechanisms presented. Dialysis of the latexes changed their properties drastically as they became unstable to coagulation. The original latexes did not change their properties over several months.

Key words Emulsion polymerization – Surfactant-free – Particle nucleation – Surface charge density – Particle morphology

Introduction

Carrying out emulsion polymerizations usually requires the presence of stabilisers imparting colloidal stability to monomer swollen polymer particles, which are the main loci of polymerization.

A surfactant-free emulsion polymerization has special attraction in the fact that stabilizing species are formed in situ during the polymerization if an initiator is used which leads to hydrophilic radicals starting the polymerization. Different types of initiators which fulfil this requirement are known; for instance potassium peroxodisulfate (KPS), 2,2′-azobis(2-amidinopropane)dihydrochloride (V-50 from Wako Chemicals), or polyethyleneglycol-azo initiators (PEGA types) [1]. Surfactant-free emulsion polymerizations in the presence of either surface-active initiators or ionic comonomers are outside the scope of this contribution. The application of PEGA initiators in heterophase polymerizations has been discussed in detail recently [2] and hence will not be considered here. In contrast to the PEGA initiators, which lead to particles being exclusively sterically stabilized, ionic initiators are considered to lead to exclusively electrostatically stabilized model colloids [3–5]. Another important feature of surfactant-free emulsion polymerizations, which is also of some practical importance, is the possibility to produce extremely monodisperse latexes if the process is controlled in a proper way [6–11].

In surfactant-free emulsion polymerizations with ionic initiators stabilization as well as destabilization is purely electrostatic. After nucleation the growth of the particle may occur not only by monomer consumption but in some cases also by particle coalescence leading to a decrease in particle concentration in the course of the polymerization as it was shown for emulsifier-free polymerizations of vinyl chloride [12] and styrene [13–16]. Consequently, the resulting particle size in a surfactant-free emulsion polymerization with ionic initiators can be considered as a result of well-balanced nucleation, growth, and coalescence processes. The term coalescence is more appropriate than coagulation as the resulting particles possess a spherical shape.

There is another exciting experimental result of surfactant-free styrene emulsion polymerization with KPS which has been known for 25 years: the formation

of particles with anomalous structures during a certain time period in the course of the polymerization. This phenomenon was extensively investigated by Wilkinson and coworkers [13, 14, 17–19]. The authors observed particles with voids (regions of less electron density) on both transmission electron microscopy (TEM) and scanning electron microscopy (SEM) pictures. They also used stereo-pair electron microscopy and confirmed the presence of voids in the polystyrene particles [18]. These investigations led to the clear conclusion that the formation of voids occurred inside each particle and is not the result of a breaking up of particle clusters [18]. In a later paper the authors concluded that anomalous regions are actually present in the particles and that their formation is a consequence of an uneven monomer distribution within the particles which is caused by the "presence of a picket of low-molecular-weight polymer originating from the nucleation and coagulation stage early on in the reaction" [14]. This group also found that in cleaned samples of such latexes, if electrolyte was added it was deposited during preparation for TEM inside the voids. In a very recently published paper [11] other authors presented TEM pictures, unfortunately without a detailed discussion, of surfactant-free polystyrene latexes prepared with KPS as initiator which clearly show regions of lower electron density inside the particles. The morphology of these particles is very similar to that observed by Wilkinson and coworkers. However, it is worthwhile pointing out that the formation of anomalous particles is not a special feature of surfactant-free polymerizations alone. In a comprehensive study of rubber latex particles by TEM at the beginning of the 1960s Rupar and Mitchell [20] observed several "abnormally" shaped particles of polystyrene as well as of polybutadiene-*co*-styrene latexes prepared in the presence of emulsifiers. These authors concluded that the presence of low-molecular-weight polymer or unreacted monomer within latex particles leads to a variety of distinct particle shapes as for instance dumbell particles, or long- and short-stem tack particles, or die- and doughnut-shaped particles. In the case of tack particles these authors believed that the deformed stem is composed of lower-molecular-weight polymer rather than the spherical head of the tack. Unfortunately, in all of these investigations no quantification of the molecular-weight regions favouring the formation of anomalous particles is given. Until today, the formation of such particles is considered to happen more or less accidentally.

In conclusion to the brief literature survey, surfactant-free emulsion polymerization has inspired continuous scientific interest in heterophase polymerization research for over 30 years. Besides the previously mentioned topics, special interest has been devoted to peculiarities of particle nucleation [15, 16, 21, 22], in situ stabilizer formation [23], and polymerization kinetics [13, 14, 24–28].

The aim of this contribution is to summarize our own experimental results of surfactant-free emulsion polymerizations of styrene started with ionic initiators (KPS and V50) with respect to two topics: particle formation as well as the development of particle and polymer properties in the course of polymerization. For particle nucleation special emphasis is placed firstly, on the persulfate decomposition as well as aqueous phase chemistry and secondly, on the chemical structure of nucleating species. The development of latex, particle and polymer properties was determined by means of comprehensive experimental measurements in the change of molecular weight distribution (MWD), particle size distribution (PSD), latex surface tension (γ), surface charge density (σ), and particle morphology in the course of the polymerization. This seems to be important as a gap in the published literature will be closed. It is worthwhile mentioning that the development of the surface charge density dependence on other polymer and particle properties is of special importance as in the surfactant-free case the initiator is responsible for both stabilization and destabilization.

It turned out, that depending on the topic (particle nucleation, chemical structure of nucleating species, and development of polymer and particle properties) different polymerization recipes are necessary in order to obtain experimental data that allow a clear interpretation. This means the experimental results have been obtained from three different recipes with respect to the monomer-to-initiator ratio and polymerization temperature.

In a third part, some properties of polystyrene model oligomers prepared by anionic polymerization will be reported with respect to particle nucleation as well as the formation of particles with anomalous morphology.

Experimental

Chemicals

Styrene, KPS 1,1-diphenylethene, *sec*-butyllithium (s-BuLi) as a 1.3 M solution in tetrahydrofuran (THF), 1,3-propanesultone, thiomalic acid, all from Sigma-Aldrich, sodium hydrogen carbonate from Fluka, and V-50 from Wako Chemicals were all used as received expect for the monomer. The THF for the anionic polymerizations was prepared and dried according to standard procedures. Deionized water was taken from a REWA HQ 5 system (18 MΩ cm^{-1}) and degassed prior to use. The monomer was distilled under reduced pressure to remove inhibitors and stored in a refrigerator. Prior to use, to check whether or not oligomers had been formed, a drop of monomer was added into an excess of methanol. Only oligomer-free monomer was used.

Emulsion polymerizations

The three different recipes used are summarized in Table 1. The polymerizations to investigate particle nucleation (recipe A) were carried out in an all-Teflon reactor adapted to a UV-vis spectrophotometer Spekol 11 (Carl Zeiss Jena, Germany) allowing on-line turbidity measurements. The conductivity and the temperature of the reaction system were also measured on-line with a conductivity

Table 1 Polymerization recipes

Ingredient	Recipe A	Recipe B	Recipe C
Water	400 ml	2000 ml	2000 ml
Styrene[a]	4.478 g (107.5 mM)	0.8957 g (4.3 mM)	91.1 g (437.35 mM)
Initiator[a]	0.2703 g (2.5 mM)[b]	3 g (5.55 mM)[c]	1.872 g (3.46 mM)[b]
$NaHCO_3$[a]	None	0/0.5 g (0/2.98 mM)[d]	0.021 g (0.125 mM)
Thiomalic acid[a]	None	None	None or 0.277 g or 1.384 g[e] (0.92 mM or 4.6 mM)
Temperature	60 °C	60 °C	70 °C
Aim	Nucleation, conductivity measurements and KPS decomposition	To investigate the chemical structure of the nucleating species	Particle and polymer properties in the course of the polymerization

[a] Molar concentrations based on aqueous phase
[b] Initiator KPS
[c] Initiator KPS and V50, respectively
[d] Final pH in absence and in presence of buffer is 2.63 and 7.20, respectively
[e] Absence of thiomalic acid run A, with 0.227 g run B, with 1.384 g run C

meter CDM83 (Radiometer, Copenhagen, Denmark) equipped with a PP1042 conductivity electrode and a T801 temperature sensor. The experimental procedure was described in detail elsewhere [15].

The polymer material for the investigations of the structure of the nucleating species was obtained from polymerizations (recipe B) in an all-glass reactor. Only the products located inside the polymer particles at the end of the polymerizations were used for the characterizations. A detailed description of the polymerization procedures with KPS as initiator and the characterization techniques employed can be found elsewhere [29]. Polymerizations with V50 instead of KPS as initiator were carried out in the same way. In order to check the reproducibility and to get enough product for the subsequent characterizations the polymerizations were repeated at least 4 times.

The polymerizations to investigate the change of latex, particle and polymer properties during the course of the polymerizations (recipe C) were carried out batchwise in a 2000-ml all-glass reactor with a heating jacket to control the polymerization temperature. The reactor was equipped with a baffle stirrer, a reflux condenser, a nitrogen inlet, and a valve on the bottom to take samples during polymerization.

The polymerizations were carried out as follows: 1930 ml water, 91.1 g styrene monomer, 0.021 g sodium hydrogen carbonate buffer, and if necessary the thiomalic acid chain-transfer agent (CTA) (either 1 or 0.2 mol % relative to styrene monomer) were charged in the reactor under stirring and purged with nitrogen gas. After at least 30 min the temperature was equilibrated (70 °C), and the reaction was started by injecting 1.872 g KPS dissolved in 70 ml degassed water. The re-heating up to 70 °C after injecting the initiator solution occurred within less than 2 min. Samples of almost 100-ml volume were taken from the bottom valve of the reactor at different polymerization times. The samples were immediately cooled in an ice bath and the solid content determined with a HR73 halogen moisture analyzer (Mettler Toledo, Giessen, Germany) at a temperature of 150 °C. The solids from this determination were also used for determination of the molecular-weight distributions. Because of this procedure it was possible to get molecular-weight data unaffected by post-polymerization processes during storage of the samples. In order to check the reproducibility the polymerization was repeated with sampling at different times. Furthermore, it was checked that the drying temperature has no influence on the molecular-weight data.

Some samples were dialysed against distilled water with Servapor dialysis tubing no. 44146 with a molecular-weight cut-off of 12,000–14,000 g mol^{-1}. Latex samples (50 ml) were dialysed against 10 l distilled water over a period of 4 weeks during which distilled water was replaced twice in 24 h.

In order to get more kinetic information calorimeter experiments with a RM200S calorimeter (ChemiSens AB, Lund, Sweden) were carried out with a 1:13.33 reduction of recipe C. A detailed description of the polymerizations in the calorimeter can be found elsewhere [2, 30].

Polymer and latex characterization

The particle size of the final latexes was analysed either by dynamic light scattering (DLS) with a Nicomp particle sizer (model 370, PSS Santa Barbara, USA) at a fixed scattering angle of 90° or by enumeration of TEM pictures. The PSDs were estimated by counting at least 700 particles per sample with an Opton TGZ3 counter from Zeiss (Oberkochen, Germany). TEM was performed on a Tesla BS 500 transmission electron microscope with an acceleration voltage of 60 kV, and SEM investigations were performed on a Zeiss DSM 940 A (Oberkochen, Germany) scanning electron microscope. The solid content of the samples for the TEM investigations was adjusted to about 0.5% relative to water. For the SEM investigations the samples were not diluted in order to see packing of the monodisperse particles. For the TEM investigations a few microlitres of the dispersion were dropped on a colodion-coated copper grid, and the water was allowed slowly to evaporate at ambient temperature (suspension preparation). The same technique was applied to prepare samples for SEM investigations. After drying these samples were sputtered with a Pd-Ir layer.

The gel permeation chromatography (GPC) analysis was performed on a P1000 pump with a UV1000 detector (λ = 260 nm) both from Thermo Separation Products with 5 μm 8 × 300 mm SDV columns with 10^6, 10^5, 10^3 Å from Polymer Standard Service in THF with a flow rate of 1 ml min^{-1} at 30 °C. The molecular weights were calculated with a calibration curve relative to PS standards.

The latex surface tension was measured with a TD1 tensiometer (Lauda, Königshofen, Germany) at 25 °C in the plate arrangement.

The number of charges per particle and the surface charge density were determined with a particle charge detector PCD-02 (Mütek, Herrsching, Germany) by measuring the streaming potential. The latex samples with a known solids content were titrated with a polyelectrolyte standard (0.1 mM polydiallyldimethylammonium-chloride solution) to determine the point of zero charge. These

titrations were carried out with at least four different latex concentrations. The number of charges per gram latex solid were calculated from the slope of the polyelectrolyte consumption versus latex concentration plot.

Matrix-assisted laser desorption ionization time-of-flight mass spectrometry (MALDI-TOF-MS) investigations were carried out with a Kratos Maldi III from Shimadzu with a linear reflectron configuration. The matrix was 1,8,9-anthracenetriol and silver trifluoroacetate was used to form the adduct. Matrix, sample, and silver trifluoroacetate were dissolved in THF with a molar ratio matrix/sample/silver salt of 700/70/1. An appropriate amount of that solution was placed on a sample holder and the THF was allowed to evaporate at ambient temperature. A two-point calibration was used with 2,5-dihydroxybenzoic acid and insulin as standards.

Elemental analysis was carried out with a EA1110 CHNSO instrument (CE Instruments). The atomic force measurements (AFM) were performed with a Nanoscope IIIa MultiMode scanning probe microscope (Digital Instruments, Inc., Santa Barbara, USA). A few drops of the dispersions were deposited on a freshly cleaved mica surface by spin-coating. After drying the samples were measured with a silicon cantilever (Nanosensors) in tapping mode with a resonance frequency of about 290 kHz.

Preparation of model oligomers

Polystyrene model oligomers, in each case with one sulfonate group per molecule, were prepared by anionic polymerization in THF with s-BuLi as initiator. THF (1000 ml) and a predetermined amount of s-BuLi (depending on the desired degree of oligomerization) were placed in a 2000-ml reaction flask and cooled to −65 °C. Styrene was condensed into the turbid yellow reaction mixture over a time period of 5 h. The monomer-to-initiator ratio was chosen in such a way that oligomers with average degrees of oligomerization of 2, 5, and 12 (samples: st02, st05, st12) were obtained, respectively. For st02, st05, and st12 the monomer/initiator solution ratio was 200 g/671.3 g, 200 g/268.5 g, and 200 g/111.8 g, respectively. Afterwards an excess of 1,1-diphenylethene was added and the colour of the reaction mixture changed from orange to red. After a reaction time of 1 h an excess of 1,3-propanesultone was added to stop the reaction. To isolate the st12 oligomers the THF solution was added into a tenfold amount of distilled water. The polymer precipitated and immediately formed a coarsely dispersed suspension. The solid was separated by filtration and dried. St02 and st05 were isolated from solution by evaporation of THF as the aqueous dispersions are too fine to separate the polymer by filtration.

Results

KPS decomposition, particle nucleation, and structure of nucleating oligomers

Initiator decomposition is the initial step in the emulsion polymerization procedure considered. The reaction starts in the aqueous phase with solution polymerization. It takes a few minutes until the first particles are detectable. This period of time is the prenucleation stage. The simplicity of recipe A and the absence of other ionic species (buffers, surfactants, etc.) make conductivity measurements in this particular case a very useful tool. Indeed, the clear detection of the onset of particle nucleation in the surfactant-free emulsion polymerization of styrene was possible for the first time by on-line conductivity measurements [15, 16]. It is interesting to point out that the conductivity–time curve reacts much earlier than optical methods and it changes its slope within 1 s due to particle nucleation. As the decomposition of KPS is already well investigated [31–33] the question arises as to whether or not it is possible to recalculate the measured conductivity curves. Furthermore, correct knowledge of the KPS decomposition is a prerequisite for a complete understanding of this particular emulsion polymerization and, in particular, particle nucleation.

The measured conductivity κ is determined by all single ionic species present, as given by Eq. (1).

$$\kappa(t) = \sum_{i=1}^{n} c_i \Lambda_{m,i} \quad . \tag{1}$$

Thus, to model the course of $\kappa(t)$ concentration, c_i, and molar ionic conductivities, $\Lambda_{m,i}$, of all ions present in the reaction mixture must be known. Note, for a mixture of electrolytes the conductivity calculated by Eq. (1) is too high, because it does not consider ionic interactions.

The mechanism of KPS decomposition derived by Kolthoff and Miller [31] leads to Eq. (2) for the change in the overall conductivity during the prenucleation stage of the polymerization (cf. Appendix for a detailed derivation and the stringent assumptions)

$$\begin{aligned}\kappa(t) = {} & \Lambda_{K^+}[K^+] + \Lambda_{S_2O_8^{2-}}\left[S_2O_8^{2-}\right] + \Lambda_{H^+}[H^+] \\ & + \Lambda_{SO_4^{2-}}\left[SO_4^{2-}\right] + \Lambda_{HSO_4^-}\left[HSO_4^-\right] \quad .\end{aligned} \tag{2}$$

To test the validity of Eq. (2) the decomposition of KPS in pure water as well as in the presence of styrene at 60 °C was investigated by conductivity measurements. The results are summarized in Fig. 1. In the case of pure water the measured conductivity–time curve can be almost exactly recalculated with a value $k_1 = 6.5 \times 10^{-6}\ s^{-1}$ which is pretty close to the value given in Ref. [31] ($k_1 = 5.02 \times 10^{-6}\ s^{-1}$). The slight difference is presumably caused by the different reactor materials: glass versus Teflon.

If the aqueous phase is saturated with styrene and a flux of styrene into the aqueous phase is maintained over the entire reaction the deviation between measured and calculated conductivity is less than 5% during the first 400 s. The good agreement was obtained with a KPS decomposition rate constant of $k_1 = 8.6 \times 10^{-5}\ s^{-1}$ which is much higher than that for the decomposition in pure water [31] ($k_1 = 5.02 \times 10^{-6}\ s^{-1}$). This is not surprising as it is well known that the decomposition of persulfate is strongly influenced by organic compounds. Factors of up to 100 compared to the decomposition in pure water have been observed in the presence of organic compounds [32].

After a reaction time of exactly 432 s the deviation between measured and calculated conductivity becomes larger and larger due to a bend in the experimental curve

which indicates a lower increase in the overall conductivity than calculated. According to Eq. (1) the reason for a lower conductivity is either a lower concentration of conducting species or a loss of mobility. A comparison of the molar conductivities of different charged species (Table 2) shows that the conductivity is governed by the protons. This assumption is supported by the experimental fact that the pH–time curve bends at exactly the same time in a direction indicating a lower increase in the proton concentration. This behaviour is highly reproducible and the bend occurs within 1 s. Based on these experimental facts the conclusion that at the time of the bend protons lose mobility is straightforward. The most likely reason is that the bend indicates the formation of a crop of particles. These particles are able to capture protons either due to specific adsorption or due to incorporation in the electric double layer thus leading to a reduction in the increase in conductivity. It is reasonable to assume that the capture of protons by particles is proportional to the total particle surface area (ND^2) where N is the particle concentration and D the particle diameter. Since the polymer concentration is at this stage very low, the turbidity, τ, scales with $\tau \propto ND^6$ and hence, the combination of on-line turbidity and on-line conductivity measurements together with a proper model to calculate the conductivity–time curve allow the change in the particle sizes just after particle nucleation to be determined according to Eq. (3) [16].

$$\frac{\tau}{\Delta\kappa} = F \cdot D^4 \quad . \tag{3}$$

In Eq. (3) F is a complex constant that is fitted from off-line measured particle sizes which is possible in later stages of the reaction and $\Delta\kappa$ is the difference between the calculated and the experimental conductivity after the bend. Knowing particle diameters and turbidities the table of scattering functions for spherical particles can be used in the reverse sense to calculate polymer concentrations and subsequently particle concentrations [15]. Quasi on-line determinations of particle size and particle concentration are possible with this procedure.

Figure 2 shows corresponding data for a polymerization according to recipe A. Note that the error connected with the application of Eq. (3) is greater the higher the transmission (decreasing time). Nevertheless, the detection and observation of particle nucleation in a surfactant-free emulsion polymerization of styrene is clear. The open symbols in Fig. 2 correspond to off-line determined particle sizes (DLS) and particle numbers, respectively, estimated by a procedure described in Ref. [15]. Although, the off-line determination of particle sizes, with the DLS equipment used, is possible at an optical transmission of 80% for the first time, and this is far away from the nucleation moment, the estimation of F in Eq. (3) is still possible. The resulting curves for D and N posses two important features. Firstly, a huge number of particles is formed within a time gap of less than 1 s and secondly, the number of particles continuously decreases just after nucleation over the entire reaction period. These results are very reasonable as Goodall et al. [13] also observed continuously decreasing particle numbers in the same concentration range

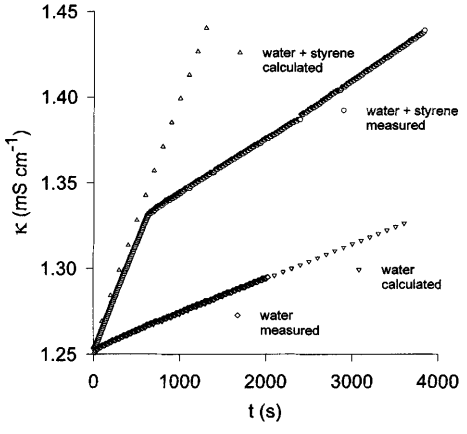

Fig. 1 Change of conductivity during the decomposition of potassium peroxodisulfate (KPS) at 60 °C in the absence and presence of styrene (recipe A)

Table 2 Molar conductivities of the different ionic species

Ion	Λ_m (m^2 S mol^{-1}) (25 °C) measured	Λ_m (m^2 S mol^{-1}) (60 °C) calculated
H^+	349.65	507.1
HSO_4^-	50	95.4
K^+	73.48	132.2
SO_4^{2-}	160	290.2
$S_2O_8^{2-}$	172	328.3

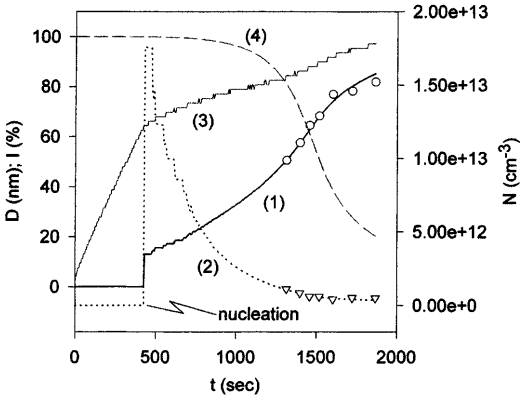

Fig. 2 On-line determination of average particle size and particle number in the surfactant-free emulsion polymerization of styrene (recipe A). *1* – average particle size (D); *open circles*: off-line particle size from dynamic light scattering (*DLS*). *2* – particle number (N); *open triangles*: off-line particle numbers. *3* – conductivity (no y-axis). *4* – optical transmission (I)

by off-line sampling starting in a later polymerization stage.

Now, the conditions at the time of nucleation (index 0) can be characterized. The prenucleation period has a duration of 431 s, nucleation takes place at a time $t_0 = 432$ s where a huge number of particles ($N_0 = 1.76 \times 10^{13}$ cm^{-3}) is formed with an average diameter of $D_0 = 13$ nm. From these values it can be concluded that each particle consists of about 7000 styrene units as a maximum value (for the calculation the density of polystyrene was used and no end groups were considered); however, this is not an unrealistic number as the total number of styrene units inside particles is 1.23×10^{17} cm^{-3} and is still lower than the saturation concentration of styrene in the aqueous phase at 60 °C (3.06×10^{18} cm^{-3}) [34]. From the total number of styrene units inside particles at nucleation it follows that the minimum amount of polymer formed up to this moment is 2.13×10^{-5} g cm^{-3}.

In conclusion, experimental conductivity–time curves of a surfactant-free emulsion polymerization of styrene initiated with KPS can be recalculated using the decomposition mechanism proposed by Kolthoff and Miller [31]. The good quality of the recalculated curves is an essential requirement for a quasi on-line determination of particle size and number as well as a quanti fication of the conditions at the time of particle nucleation. The estimated data supports a nucleation mechanism according to classical nucleation theory [16, 35] which requires an aggregation of more than one chain compared to a single chain precipitation nucleation mechanism [21].

Important questions of particle nucleation are not answered by the results described so far. Firstly, what is the chain length of the nucleating species? Secondly, what is the chemical nature of the end groups of the nucleating species? Both questions are connected with each other as in surfactant-free emulsion polymerizations the solubility of the products formed during the prenucleation stage is crucial for particle nucleation. Answers to both questions are not easy as the initiation of a polymerization reaction in aqueous media by sulfate ion radicals is only a side reaction as approximately 70% of all radicals react with water or organic recipe components. Consequently, end groups other than sulfate have also been detected on polystyrene particles, for instance carboxyl and hydroxyl groups [29, 36–40]; however, there is dispute about the mechanism of the formation of carboxyl and hydroxyl end groups in the literature [5, 29, 37].

In order to investigate the chemical structure of the nucleating species it is necessary to analyse the polymer inside the particles. MALDI-TOF-MS is a powerful tool to investigate both the MWD and the end group compositions of polymer molecules [41]; however, the molecular weight must be less than 10^4 g mol^{-1} in order to be successful. To reduce the molecular weight of the polymer formed inside the particles recipe B (cf. Table 1) was used with a monomer concentration that corresponds almost to the saturation concentration of styrene in water at the polymerization temperature [34]. Because of this, the monomer starvation regime follows immediately after particle nucleation and hence, the molecular weight is restricted to the desired level [29]. An interesting question in this context is whether or not different initiators lead to different PSD and end group compositions? KPS and V50 were used according to recipe B in order to see the influence of charge as well as the influence of the chemical nature of the radicals. As there are some results indicating an influence of buffer on the nature of charged groups [5] polymerizations were carried out in the absence as well as in the presence of sodium hydrogen carbonate buffer. The results depicted in Figs. 3 and 4 clearly show an influence of

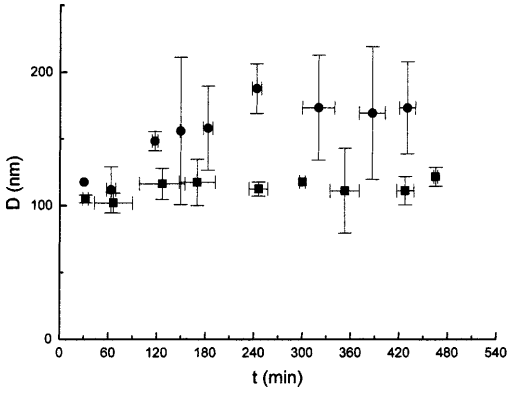

Fig. 3 Development of the average particle size (DLS) in the course of the polymerization with KPS (*filled circles*) and 2,2′-azobis (2-amidinopropane)dihydrochloride (*V50*) (*filled squares*); recipe B without buffer; the *lines* indicate the standard deviations (average standard deviations for KPS 31.7 nm and V50 13.7 nm)

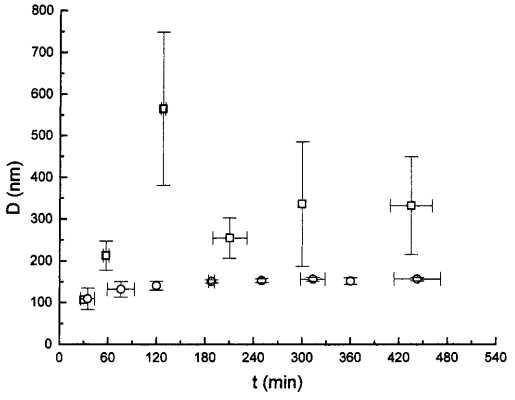

Fig. 4 Development of the average particle size (DLS) in the course of the polymerization with KPS (*open circles*) and V50 (*open squares*); recipe B with buffer; the *lines* indicate the standard deviations (average standard deviations for KPS 10.0 nm and V50 106.5 nm)

the initiator as well as of the presence or absence of buffer on the development of D. In the absence of buffer V50 leads to slightly smaller particles than KPS and the data scatter more than in the case of KPS (cf. Fig. 3). The situation changes to the opposite in the presence of buffer (cf. Fig. 4) where V50 leads to much larger particles and a much stronger scatter of the data compared to the situation where no buffer was used. In contrast, KPS leads to slightly larger particles and to a lower scatter in the presence of buffer. For KPS these results can be explained with possibly fewer side reactions in the presence of buffer leading to a lower scatter and the slightly increased ionic strength possibly increases the average particle size. The considerably larger particles in the case of V50 with buffer may be explained by a basic hydrolysis of the amidinium groups leading to free base and hence stability is lost due to a reduction in the number of charges.

Parts of MALDI-TOF-MS spectra of two polystyrene samples are shown in Fig. 5. Curve A corresponds to a sample prepared by a radical polymerization according to recipe B with V50 as initiator (2L49) and curve B represents a model oligomer (st05). The MALDI-TOF-MS spectra of st05 is characterized by one single peak for each chain length whereas for 2L49 the signal of each chain length is composed of at least five separate peaks. An even higher number of separate peaks results as surfactant-free emulsion polymerization with KPS as initiator is conducted [29]. Figure 5 clearly illustrates the occurrence of more than one end group combination due to side reactions in aqueous heterophase polymerizations. The measured residual mass of st05 is 262.6 g mol^{-1} which corresponds exactly to the theoretical value (262.3 g mol^{-1}). The determination of the residual masses or end-group combinations for 2L49 leads to the data summarized in Table 3. Note that the data scatter slightly more than for KPS as initiator [29]. Nevertheless an important result is clear: there are more than two end-group combinations indicating carbon radical side reactions during heterophase polymerizations. It is reasonable to consider two end groups as the ideal case since it is very likely that either the amidinopropane hydrochloride residue or the amidine (free base) residue may form an end group or fly, respectively. Even MALDI-TOF-MS investigations with pure V50 gave no clear decision which species fly. All results indicate that it is more than one species. The peaks with the highest intensities in the MALDI-TOF-MS spectra correspond to the residual masses of about 70 and 90 g mol^{-1}, respectively. The attempt to assign end groups to the residual masses gives some evidence for side reactions leading to hydroxyl and hydrogen radicals (cf. Table 3). The MALDI-TOF-MS results are supported by elemental analysis data, FT-IR measurements, and NMR investigations. All methods confirm the presence of other groups besides those arising from an ideal initiator decomposition. For example, elemental analysis of the polymers initiated with V50 (recipe B) indicates an oxygen content of up to 0.5%. If oligomers with hydroxyl end groups are in the vicinity of ionic end groups it is very likely that the former will nucleate with shorter chain lengths. Furthermore, the possibility of mixed nucleation can no longer be excluded. A carbon radical, besides starting the polymerization, may react with water [1, 42] leading to a hydroxyl radical which can either react with a monomer molecule or recombine with another hydroxyl radical to form hydrogen peroxide. In a subsequent reaction the hydrogen peroxide can oxidize hydroxyl end groups to carboxylic acid end groups. The

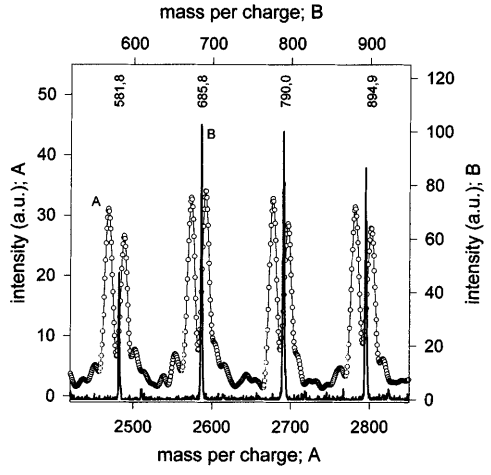

Fig. 5 Comparison of the matrix-assisted laser description ionization time-of-flight mass spectrometry spectrum of the polymer inside the final latex particles for polymerization according to recipe B started with V50 in the absence of buffer (*curve A*) with the model oligomer st05 (*curve B*)

Table 3 Residual masses and end-group combination of 2L49

M_{res} (g mol^{-1})[a]	End group combination	M_{res}^{th} (g mol^{-1})[b]
−0.32 ± 1.21	A—Am[c]	−2
	H—H	+2
32.65 ± 2.57	Am—Am	34
	Am—OH	34
	HO—OH	34
	H—COOH[d]	33
50.28 ± 1.71	Am—COOH	49
	HO—COOH	49
69.50 ± 0.84	A—A	66
	HOOC—COOH	64
88.67 ± 1.27	A—OH	93
	A—H	86

[a] Residual mass observed experimentally
[b] Calculated residual mass
[c] Am – amidinopropane dihydrochloride residue; A – amidine residue
[d] The mass of the COOH group for the calculations is 32 g mol^{-1} as this group is the result of the oxidation of a CH or CH_2 group

influence of different end groups on nucleation must be a matter of further investigations as the chemical nature of end groups determines the solubility and hence the nucleation behaviour of oligomers.

Change of latex, particle and polymer properties in the course of polymerization[1]

Some introductory remarks are necessary as experimental results are presented which were obtained without trying to remove the monomer or to clean the latexes after polymerization. To investigate the latex in its original state is crucial in order to discover important features of the particular system. Although the latexes contained monomer during storage, repeated particle size analysis with DLS and TEM after 10 months gave identical results within an error of less than 7% with respect to the first measurements. Also morphological features of the latex particles remained unchanged; however dialysis changes latex properties very drastically and leads to coagulation. Hence, the presence of monomer and water-soluble reaction products preserves latex properties over a long period of time. These findings confirm the fact that during surfactant-free emulsion polymerization the whole system develops in such a way that at the end a minimum in free energy as well as a stable latex results. Consequently, disruptions by removing components lead to a loss in stability.

A comparison of the overall reaction kinetics (recipe C without thiomalic acid) determined either by calorimetry or by gravimetric analysis of samples is shown in Fig. 6. The agreement is rather good as one has to take into consideration the fact that the calorimetric experiments and the standard polymerizations were carried out in reactors of different material and size. The reaction rate profile is characterized by a strong gel peak, and after 8 h the final conversion is well above 90%.

Figure 7a and b shows the development of the PSD and MWD characteristics, respectively, during the entire polymerization (recipe C without thiomalic acid) and illustrate at the same time the reproducibility (two

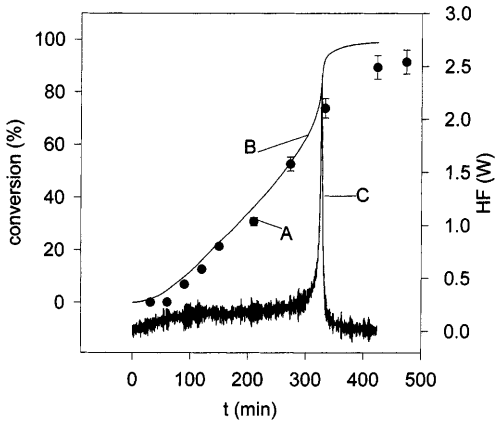

Fig. 6 Kinetics of surfactant-free emulsion polymerization of styrene (recipe C). *A* – conversion estimated from gravimetric analysis of samples. *B* – conversion from on-line calorimetric data. *C* – heat flow (rate of polymerization) from calorimetric measurements

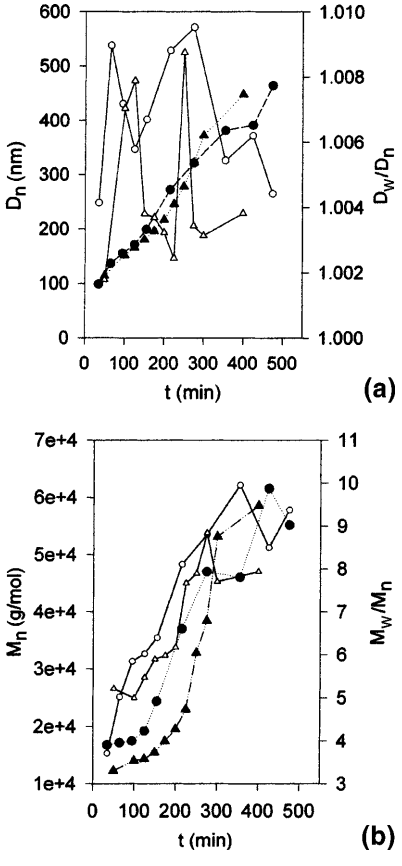

Fig. 7 a Change in the number-average particle diameter (*filled symbols*) and of the polydispersity ratio D_w/D_n (*open symbols*) with polymerization time (recipe C, without thiomalic acid); two repeats. **b** Change in the number-average molecular weight (*filled symbols*) and of the polydispersity ratio M_w/M_n (*open symbols*) with polymerization time (recipe C, without thiomalic acid); two repeats

[1] During a 2 week period two students jointly carried out their first emulsion polymerization according to recipe C in order to prepare monodisperse particles. They took ten samples over the whole duration to get to know different methods available in our laboratory. On the TEM pictures of sample 1–7 (30–273 min after the start, respectively) anomalous particles appeared which, however, disappeared again at longer polymerization times. Two attempts to reproduce these results failed. In comparison to the students' results the repeated runs resulted in polymers with a up to a factor of 3 higher molecular weight. The conclusion was that in the students' run some CTA (perhaps some lubricant from the stirrer dropped from the shaft into the reactions mixture) was accidentally present. Now it was straightforward to carry out polymerizations in the presence of CTA in order to get anomalous particles. Indeed, this was successful.

repeats are shown). Average particle size as well as average molecular weight increase with polymerization time. D_w/D_n never exceeds a value of 1.01 indicating that the PSD is very monodisperse. Although both repeats show a similar course it is more realistic to assume that D_w/D_n is almost constant within experimental error. In contrast to the PSD M_w/M_n increases during the entire reaction, ending with a value of about 9 which indicates a very broad MWD. Comparing Fig. 7a and b it is interesting to note, that the particle size seems to be better reproducible than the molecular weight.

Another interesting result is the change in the latex surface tension (with respect to air) with polymerization time (cf. Fig. 8). There is an overall increase starting from values of about 40 mN m^{-1} up to about 70 mN m^{-1} for the final latexes. The value of the first sample is surprisingly high as one would still expect free monomer at this low conversion and hence a surface tension of some 32 mN m^{-1} which is the value measured for styrene to air; however, the values are much higher and are in agreement with the fact that no free monomer phase is visible. The swelling capacity of the particles is obviously drastically increased perhaps due to the low molecular weight. Furthermore, the increase in γ is not linear but oscillates and resembles the behaviour of some continuous polymerizations [43–46]. These oscillations indicate a reverse oscillation in the concentration of surface-active oligomers in water. As the reproducibility between both repeats is not that bad one may speculate whether there is regularity behind it: further investigations are necessary. Latex surface tensions between 50 and 70 mN m^{-1} were also measured in surfactant-free styrene polymerizations by Rjabova et al. [23]. Note, however, that all measurements were done at room temperature which is almost 50 degrees below the polymerization temperature. Consequently, on-line measurements directly during the reaction are necessary to draw conclusions with respect to the polymerization mechanism.

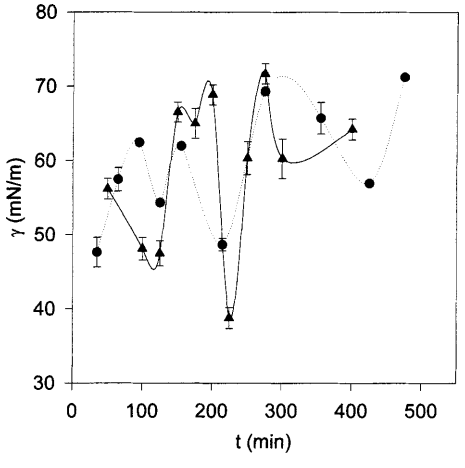

Fig. 8 Change in latex surface tension (γ) with polymerization time (recipe C, without thiomalic acid); two repeats

Another example of a latex property which can only be determined in the original samples is the number of charges per latex particle as the dialysed samples were unstable. The data depicted in Fig. 9a and b describe the development of n_L and σ during the polymerization. The measured curves are very reasonable and the reproducibility is quite good, indicated by the two repeats. The method itself has a reproducibility for latexes of the order of a few percent [47]. It is possible to compare these results with scaling laws of n_L and σ with average particle sizes and average molecular weights, respectively, as all reaction products are still present. In the particular reaction system considered the charges are only the result of initiator decomposition and subsequent initiation of chain growth. Hence, n_L and σ are controlled by three parameters: particle concentration, average particle size and average molecular weight. Equations (4) and (5) describe these dependencies, where d_P is the polymer density, N_A is Avogadro's constant, f_T is a factor that considers whether the termination is by combination ($f_T = 2$) or by disproportionation ($f_T = 1$), f_{CEG} is a

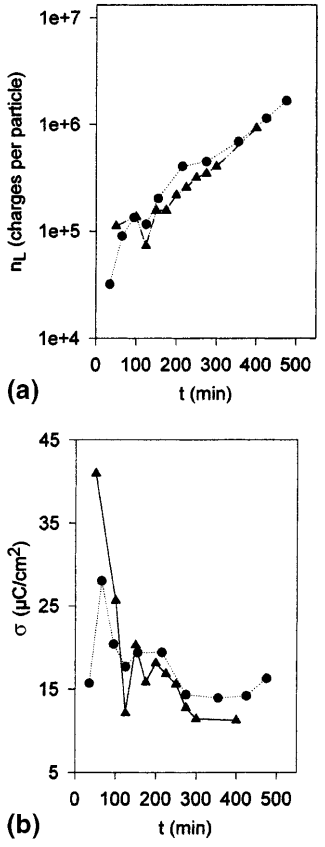

Fig. 9 a Change in charges per particle with polymerization time (recipe C, without thiomalic acid); two repeats. **b** Change in surface charge density with polymerization time (recipe C, without thiomalic acid); two repeats

factor taking into account the fact that uncharged radicals can also start chain growth even in the case of ionic initiators ($f_{CEG} \leq 1$), F is the Faraday equivalent, D is an average particle size, and M is an average molecular weight.

$$n_L = f_T \cdot f_{CEG} \cdot d_p \cdot N_A \cdot \frac{\pi D^3}{6M} \quad (4)$$

$$\sigma = \frac{F}{N_A} \cdot \frac{n_L}{\pi D^2} = f_T \cdot f_{CEG} \cdot d_p \cdot \frac{F}{6} \cdot \frac{D}{M} \quad . \quad (5)$$

Recombination of two growing radicals dominates chain termination in the radical polymerization of styrene [48, 49] and, hence f_T is 2. Furthermore, if f_{CEG} is assumed to be 1 the slope of the $n_L \propto D^3 M^{-1}$ relation should be 664.7 g mol^{-3}. The data depicted in Fig. 10a agree well with the scaling behaviour of n_L according to Eq. (4). Also, the reproducibility is excellent, Figure 10a and b was generated with D values from DLS measurements and number-average molecular weight values. The choice of an average particle size is not that critical as the PSD is very narrow. In contrast, problems arise with respect to the average molecular weight as the MWD is very broad. Consequently, the data in Fig. 10b scatter much more, but still indicate a linear relation. A better relation is obtained if instead of M_n the weight-average molecular weight is used [50]. The slopes of the straight lines in Fig. 10a (255 and 279 g mol^{-1} nm^{-3}) are more than a factor of 2 less than the theoretical value. This indicates that either f_T is less than 2 or, what is more probable, that f_{CEG} is less than 1. An f_{CEG} value less than 1 confirms the MALDI-TOF-MS data that shows the presence of uncharged end groups.

TEM pictures of all latex samples investigated so far (recipes A, B, and C) did not show any unusual morphology (anomalous particles). To test the influence of the molecular weight, according to the observations of Rupar and Mitchell [20], polymerizations were carried out in the presence of water-soluble CTA (thiomalic acid). Figure 11a–c shows some changes caused by the presence of thiomalic acid during the polymerization. As expected the molecular weight decreases with increasing amount of CTA (cf. Fig. 11a). The effect of thiomalic acid on γ is very pronounced, with increasing concentration the intensity of the oscillations as well as γ decrease (cf. Fig. 11b). Thiomalic acid obviously leads to an enhanced formation of water-soluble surface-active oligomers. A higher concentration of these oligomers has an influence on nucleation and hence on the development of the particle size during the polymerization. Increasing amounts of CTA lead to an increase in D_V (cf. Fig. 11c). The same is true, although to a much lower extent, for particle sizes determined by enumerating TEM pictures. Moreover, TEM pictures reveal that the PSD is much broader. Maximum D_w/D_n values of about 2 were estimated for both runs with thiomalic acid. For example, during run B with 0.2 mol % CTA relative to styrene (curve B in Fig. 11) D_w/D_n decreases continuously from a starting value of 1.98 to 1.05 at the end of the polymerization. Conclusions with respect to nucleation in the presence of a water-soluble CTA are straightforward. The very broad PSD indicates that nucleation takes place at different moments during the polymerization. This is very reasonable since in the presence of a water-soluble CTA many more water-soluble oligomers are formed and, if the CTA concentration is high enough, they are formed over the whole duration of the reaction.

Furthermore, the presence of higher amounts of CTA has an influence on the rate of the polymerization. Without CTA the gel peak occurs after a polymerization time of 330 min. In the presence of 0.2 mol % thiomalic acid relative to styrene the gel peak occurs after 410 min and with 1 mol % CTA the conversion after 8 h is only about 30%. Another strange effect of CTA is that on particle morphology. Anomalous particles with a chestnut-like appearance are observed on TEM pictures of samples from all runs in the presence of CTA (runs B, C, and D, cf. Fig. 11). Thus, the occurrence of these chestnut particles is strongly correlated with the molecular weight distribution. Although a detailed knowledge of that correlation is still missing, it is clear that a considerable number of polymer molecules with a

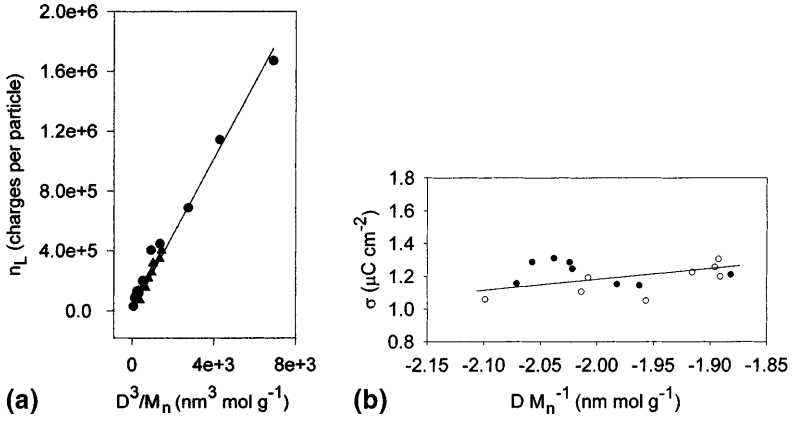

Fig. 10 a Dependence of the number of charges per particle on $D^3M_n^{-1}$ (recipe C, without thiomalic acid); two repeats. **b** Dependence of the surface charge density on DM_n^{-1} (recipe C, without thiomalic acid); two repeats

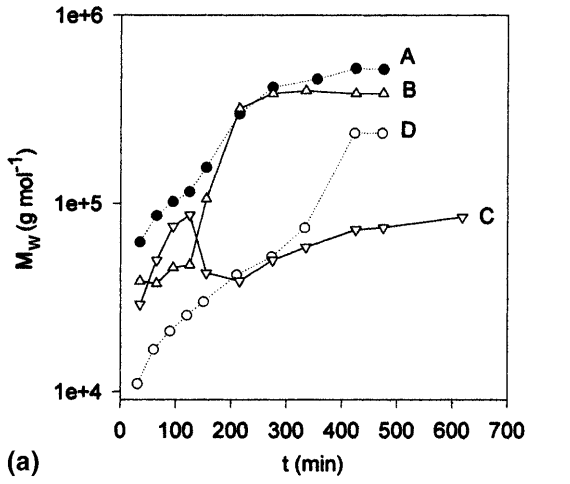

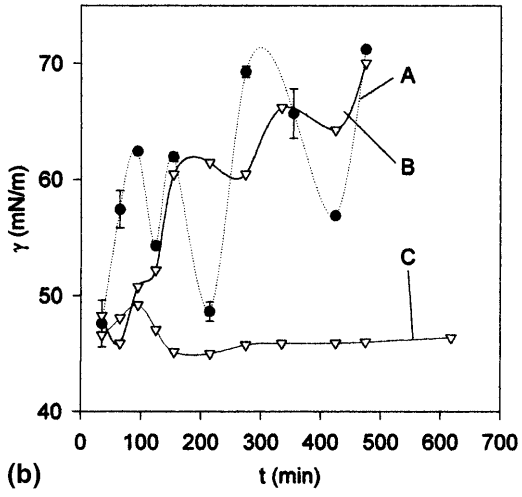

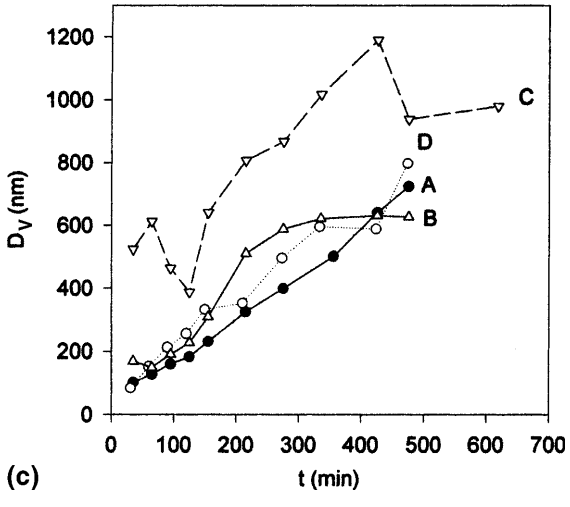

molecular weight lower than 10^4 g mol^{-1} must be present. Another prerequisite for the formation of chestnut structures is a certain chain mobility inside the particles due to swelling with residual monomer or organic solvents. However, note that with organic

◀

Fig. 11 **a** Change in the weight-average molecular weight with polymerization time (recipe C) in the presence of chain transfer agents (*CTA*). *A* – without CTA. *B* – with 0.2 mol % thiomalic acid relative to styrene. *C* – with 1 mol % thiomalic acid relative to styrene. *D* – unknown CTA. **b** Change in the latex surface tension with polymerization time (recipe C) in the presence of CTAs. *A* – without CTA. *B* – with 0.2 mol % thiomalic acid relative to styrene. *C* – with 1 mol % thiomalic acid relative to styrene. **c** Change in volume-average diameter from DLS with polymerization time (recipe C) in the presence of CTAs. *A* – without CTA. *B* – with 0.2 mol % thiomalic acid relative to styrene. *C* – with 1 mol % thiomalic acid relative to styrene. *D* – unknown CTA

solvents water also comes into the particles. For instance, water has a solubility in styrene at 51 °C of 0.123% [34]. Thus, the formation of chestnut particles during a polymerization at lower conversions is more likely than at the end of the polymerization. Indeed, in runs B and D, where the polymerization was completed, chestnut particles disappear at higher conversions, whereas in run C due to the lower final conversion anomalous particles were observed in all samples. The same behaviour was also observed by Goodall et al. [13]. Run D allows a detailed characterization of the anomalous particles as the PSD is narrow. The development of the size of the low-electron-density regions ($D_{n,hole}$) with the development of M_n and M_w in relation to monomer conversion is compared in Fig. 13a. It is clear that as the molecular weight exceeds a certain value the anomalous regions disappear. Another interesting relation exists between $D_{n,hole}$ and the polydispersity index D_w/D_n (cf. Fig. 13b). The appearance of holes leads to an increase in D_w/D_n. It is interestingly to note that the polydispersity ratio of the anomalous regions follows the course of D_w/D_n. If the holes disappear, the PSD becomes extremely monodisperse. A SEM picture of well-ordered layers of monodisperse polystyrene particles (recipe C, run D) is shown in Fig. 14.

Influence of dialysis of latex, particle and polymer properties

As already mentioned, dialysis has a devastating effect on latex stability. From ten samples prepared in the absence of thiomalic acid six samples were coagulated during dialysis and four within a few days after dialysis. Latexes prepared in the presence of thiomalic acid were stable for about 2 months after dialysis at room temperature. Besides stability, other latex, particle and polymer properties change during dialysis. Surface charge densities drop below 10 μC cm^{-2} which is in the usual range for surfactant-free systems [7, 14, 38]. Likewise, after dialysis all γ values drop. The first five samples of run A and all samples of run C drop into a ran between 30 and 20 mN m^{-1} which is extremely low. γ values for later samples of run A are between 40 and

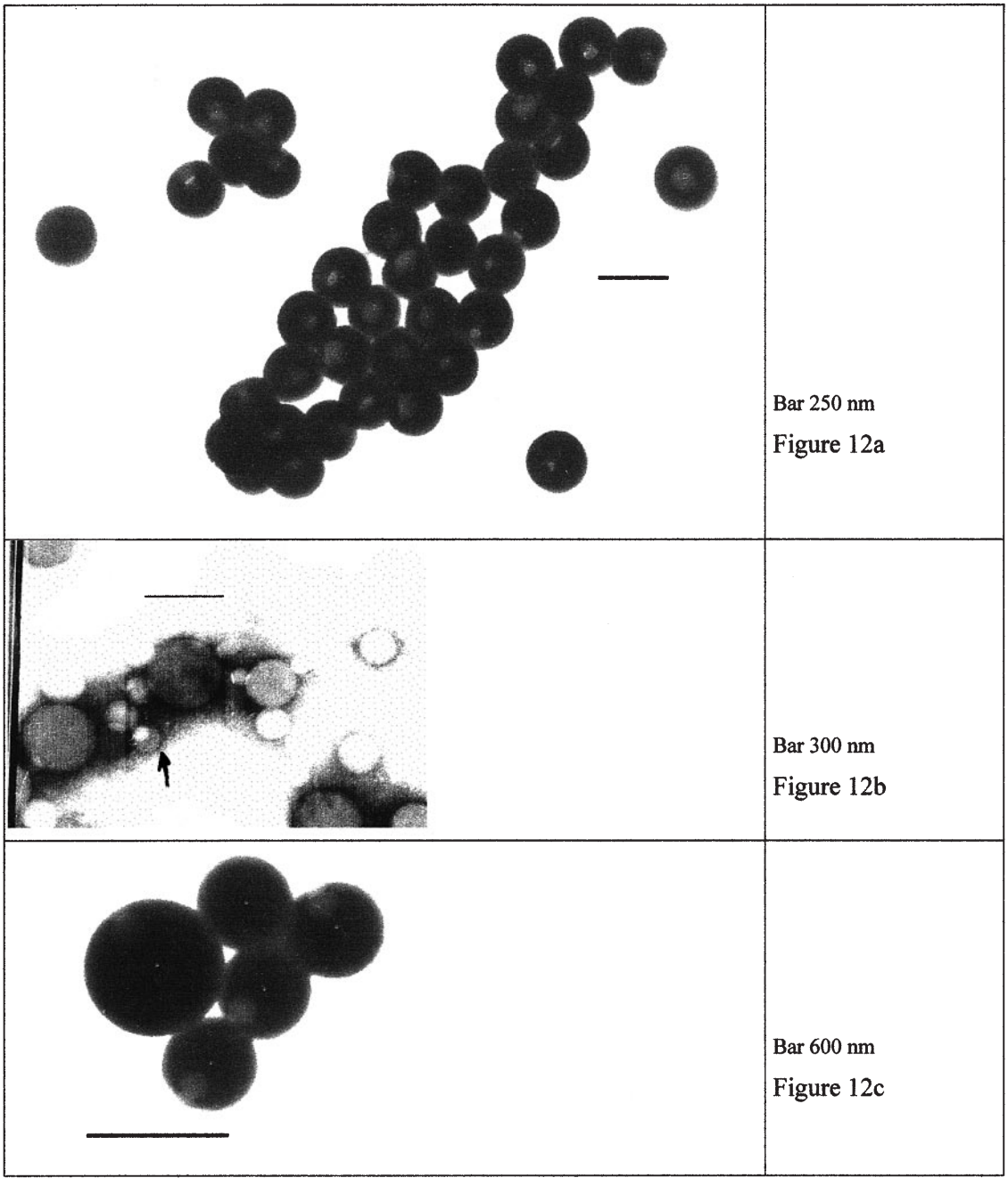

Fig. 12a–c Transmission electron microscopy (*TEM*) picture of anomalous particles. **a** recipe C (Min D unknown CTA) sampling time 90 min, **b** recipe C with 0.2 mol % thiomalic acid, sampling time 35 min, **c** recipe C with 1.0 mol % thiomalic acid, sampling time 335 min

60 mN m^{-1} but are always lower than for the original samples. A possible explanation for the decrease in γ can be found if one assumes that upon dialysis some highly surface active components from inside the particles have been released into the aqueous phase. These highly surface active components are very likely to be terminated with hydroxyls if a similar behaviour is assumed as in the case of alkyl sulfates and the corresponding alcohols [51]. For the latexes without thiomalic acid all properties related to PSD and to MWD remain unchanged. In contrast all of these properties change for run C (recipe C, in the presence of 1 mol % thiomalic acid relative for styrene). M_n decreases as well as D_v from DLS but the particle size determined from TEM pictures increases. These particles are obviously swollen

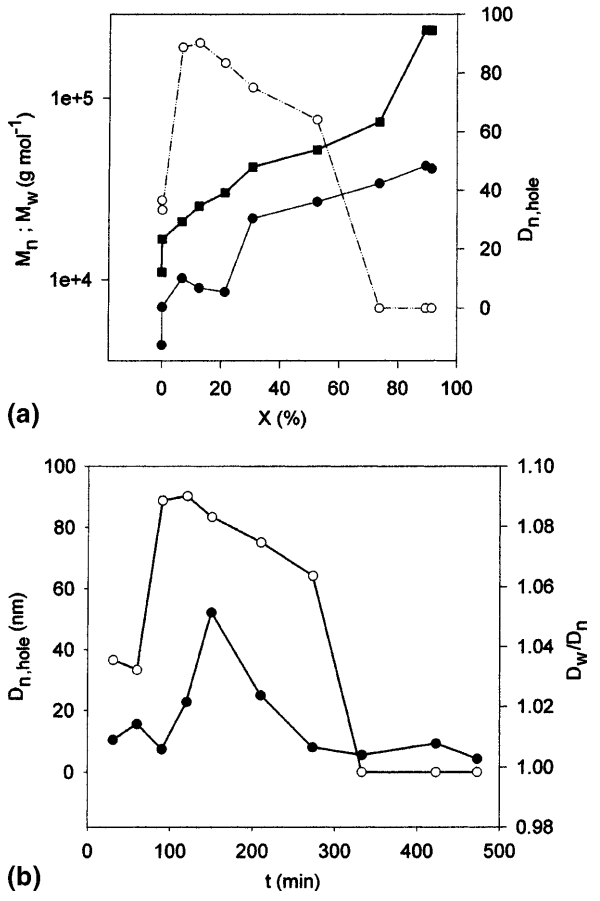

Fig. 13 **a** Change in M_n (*filled circles*), M_w (*filled squares*), and $D_{n,hole}$ (*open circles*) with conversion; recipe C run D. **b** Change in $D_{n,hole}$ (*open circles*) and D_w/D_n (*filled circles*) with polymerisation time; recipe C run D

with water and hence, may change their morphology with changing conditions in the continuous phase. For example, increasing temperature leads to a greater swelling indicated by an increase in the particle diameters measured with DLS.[2]

Dispersions of model oligomers

In the context of this contribution model oligomers are very useful with respect to investigations of particle nucleation as well as of particle morphology. Note, that the oligomers prepared have two different end groups: a sec-butyl and a propyl sulfonate end group. MALDI-TOF-MS data reveal that their chemical structure is almost perfect (cf. Fig. 5) as the theoretically expected masses of end groups have been detected for both the precursor oligomers and the sulfonated oligomers: 134.2 and 262.3 g mol^{-1}, respectively. The polydispersity M_w/M_n, determined for the precursor oligomers, is 1.62 for st02 and 1.11 for st05.

All model oligomers are practically insoluble in water but form dispersions after contact with water. Dispersions are more easily formed the lower the average molecular weight. Input of mechanical energy (high-pressure homogenizer) or ultrasound leads to the formation of dispersions with average particle sizes well below 1 μm. DLS reveals quite broad distributions with average particle sizes between 100 and 300 nm.

The TEM pictures in Fig. 15a show typical morphologies of these dispersions. The particles are not spherical and resemble broken pieces with phase-separated structures rather than ordinary latex particles. However, the situation changes completely when these dispersions are exposed to organic solvents which are able to swell the oligomer particles. Swelling leads to a complete reorganization of the dispersed particles as shape, morphology, average size, and size distribution change. The starting st12 dispersion in water had a solids content of 0.5% and an average particle size D_V = 250 nm. Upon swelling with THF and toluene (volume ratio dispersion/swelling agent 5/1) D_V increases to 400 and 456 nm, respectively. Figure 15b, c and d illustrates the changes with the help of TEM pictures. At a glance the oligomer particles resemble ordinary latexes, however, with an extremely broad PSD. Figure 15b shows a nice but accidental arrangement of the drying particles on the TEM grid. This effect is named "crystallization of opals from polydisperse nanoparticles" and has been known for many years for latex particles [20] as well as for inorganic colloids [52]. TEM pictures in Fig. 15c and d reveal that upon swelling st12 forms anomalous particles. A particle in the centre of the opal in Fig. 15c shows both a die shape and less electron dense regions. It appears as if the left particle in Fig. 15d has been shot through the centre. These results confirm that the formation of anomalous structures requires a certain chain mobility which is given to the particular system by the oligomers in the presence of swelling agents.

Investigating model oligomers with respect to particle nucleation in the aqueous styrene emulsion polymerizations leads to an important conclusion. It confirms the experimental fact obtained with recipe A that the concentration of nucleating species is extremely low. All attempts to isolate water-soluble components from the oligomer dispersions in amounts that are large enough to handle failed. Nevertheless, surface tension measurements confirm that water-soluble surface-active components are present. Figure 16 shows γ–ln c plots for all three oligomers. The plots have been obtained by feeding a known amount of dispersion with a given solid content into water. The concentration corresponds to the solid content of the diluted dispersion and does not

[2] For sample 3 of run C (recipe C) D_V continuously increases between 25 and 60 °C from 427 to 539 nm

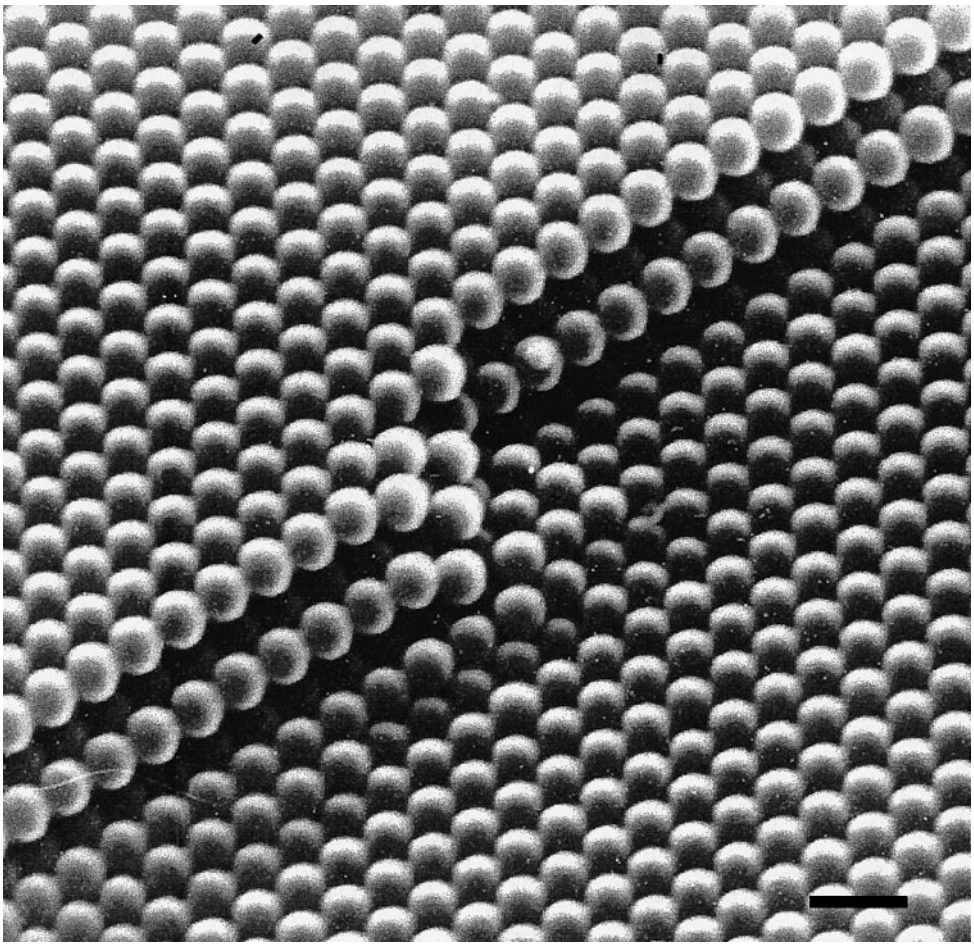

Fig. 14 Scanning electron microscopy picture of the final latex; recipe C run D

represent the surface-active, soluble components. Hence, the apparent critical micelle concentrations (cmc) cannot be compared directly as the real concentration of the solute is unknown. The shift of the apparent cmc with increasing oligomer chain length to higher concentrations is reasonable as the amount of soluble components in the oligomer dispersions should decrease. The increase in γ at the cmc with increasing oligomer chain length is an indication for a composition shift in the water-soluble components. The model oligomer dispersions represent an interesting system due to the common presence of single oligomer molecules, micelles, and particles. One may consider this as a model system for aggregation nucleation as discussed earlier.

Discussion and conclusions

Surfactant-free emulsion polymerizations are today still a field of exciting investigations. A simple recipe with only three components (water, hydrophobic monomer, hydrophilic initiator) offers ideal conditions to investigate basic phenomena with respect to particle nucleation, particle stabilization, and particle morphology. On the other hand, it is possible to investigate by gradual addition of more components their particular influence on the whole reaction system.

With respect to particle nucleation, on-line turbidity together with on-line conductivity measurements offer in the case of surfactant-free emulsion polymerization the unique possibility to clearly detect the nucleation moment. Furthermore, it is possible to estimate the nucleation conditions with respect to D_0 and N_0. The experiments clearly show that, firstly, N jumps at the moment of nucleation within 1 s to almost 2×10^{13} cm^{-3} and, secondly, that the particles consist of more than one chain. Hence, these results support an aggregation nucleation mechanism according to classical nucleation theory [16]. Further support for this mechanism arises from investigations of model oligomer dispersions where single oligomer molecules coexist with micelles and particles.

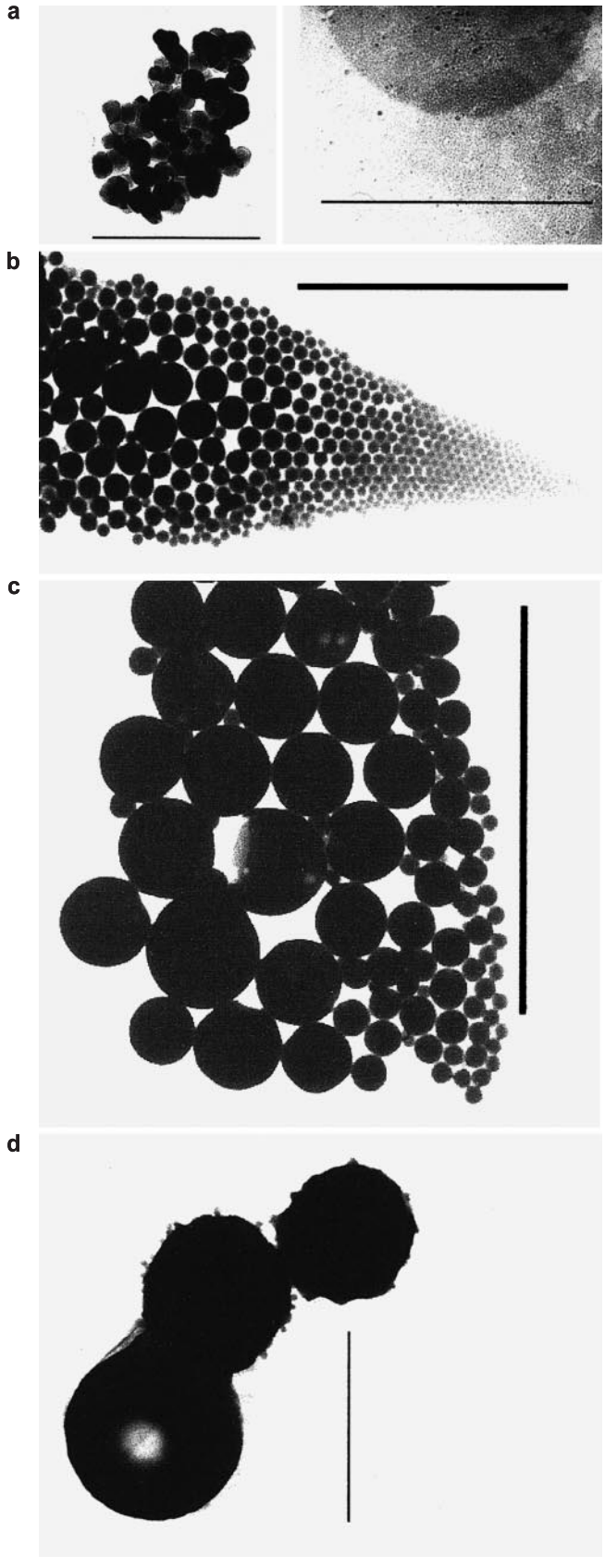

Fig. 15 TEM pictures of **a** a st12 dispersion in water (the *bars* indicate 350 nm), **b** an aqueous st12 dispersion swollen with tetrahydrofuran (*THF*) (the bar indicates 7 μm), **c** an aqueous st12 dispersions swollen with THF (the bar indicates 7 μm), and **d** an aqueous st12 dispersion swollen with toluene (the bar indicates 2 μm)

Another important investigation in order to clarify the nucleation mechanism, which is also only possible in the surfactant-free case, is the determination of the chemical structure of the polymer end groups. If emulsifiers are present, either the resulting molecular weights are too high or their presence disturbs the investigations. By means of elemental analysis and MALDI-TOF-MS investigations it turned out that besides end groups arising from free primary radicals the polymers also possess groups arising from both initiation reactions with other radicals and side reactions. Experimental evidence has been found in the case of V50 as initiator for amidinopropane dihydrochloride, amidine, hydroxyl, carboxylic acid, and hydrogen end groups. Now it is clear that not only sulfate ion radicals lead to unexpected end groups but also carbon radicals.

Ionic initiators in surfactant-free emulsion polymerization are responsible for both stability and instability. Hence, knowledge of the development of the number of charges per particle as well as of surface charge density in the course of the polymerization is crucial for a better understanding. Determination of the number of charges in the original samples confirms the expected scaling behaviour $n_L \propto D^3 M^{-1}$ as well as $\sigma \propto DM^{-1}$.

The extension of the standard recipe (three components) by adding a CTA leads not only to an expected decrease in the average molecular weight but also to the appearance of particles with less electron dense regions on TEM pictures. Similar structures were observed on TEM pictures of model oligomer dispersions after exposure to a swelling agent. Consequently, formation

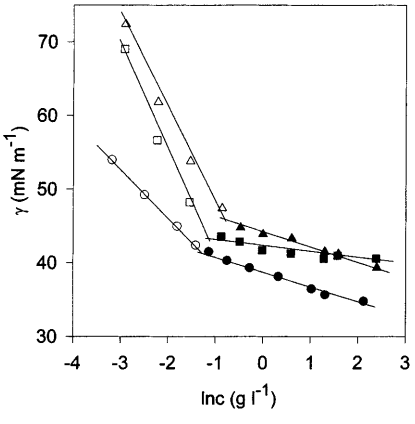

Fig. 16 Surface tension (γ) versus concentration plot for oligomer dispersions st02 (*open* and *filled circles*), st05 (*open* and *filled squares*); st12 (*open* and *filled triangles*) at 25 °C

of such anomalously shaped particles requires a certain chain mobility which is realized by a low enough molecular weight chain together with the presence of a swelling agent. The swelling agent acts as a monomer during the polymerization or as an organic solvent in the case of the model oligomer dispersions. The driving force for this ordering effect is a minimization of the free energy similar to the variety of phase separations observed either in block copolymer melts or solutions [53]. The mobility of the chains or a part of the chains near the hydrophilic head inside the particles is high enough that a phase separation into hydrophilic and hydrophobic regions takes place. The lower the molecular weight the higher the number of hydrophilic head groups for a given average particle size (cf. Eq. (4) or n_L scaling law). The increase in the interfacial area of doughnut- or die-shaped particles compared to a sphere is driven by a higher number of hydrophilic head groups which tend to maximize their distance to each other. The dissolution of the particles is prevented by the hydrophobic interaction or by entanglements of the tails if their length is above a critical value. Consequently, the increase in the interface is realized by the formation of indentations. There are some preliminary results of light-scattering investigations that support the existence of these depressions in the dispersed state. So, the AFM

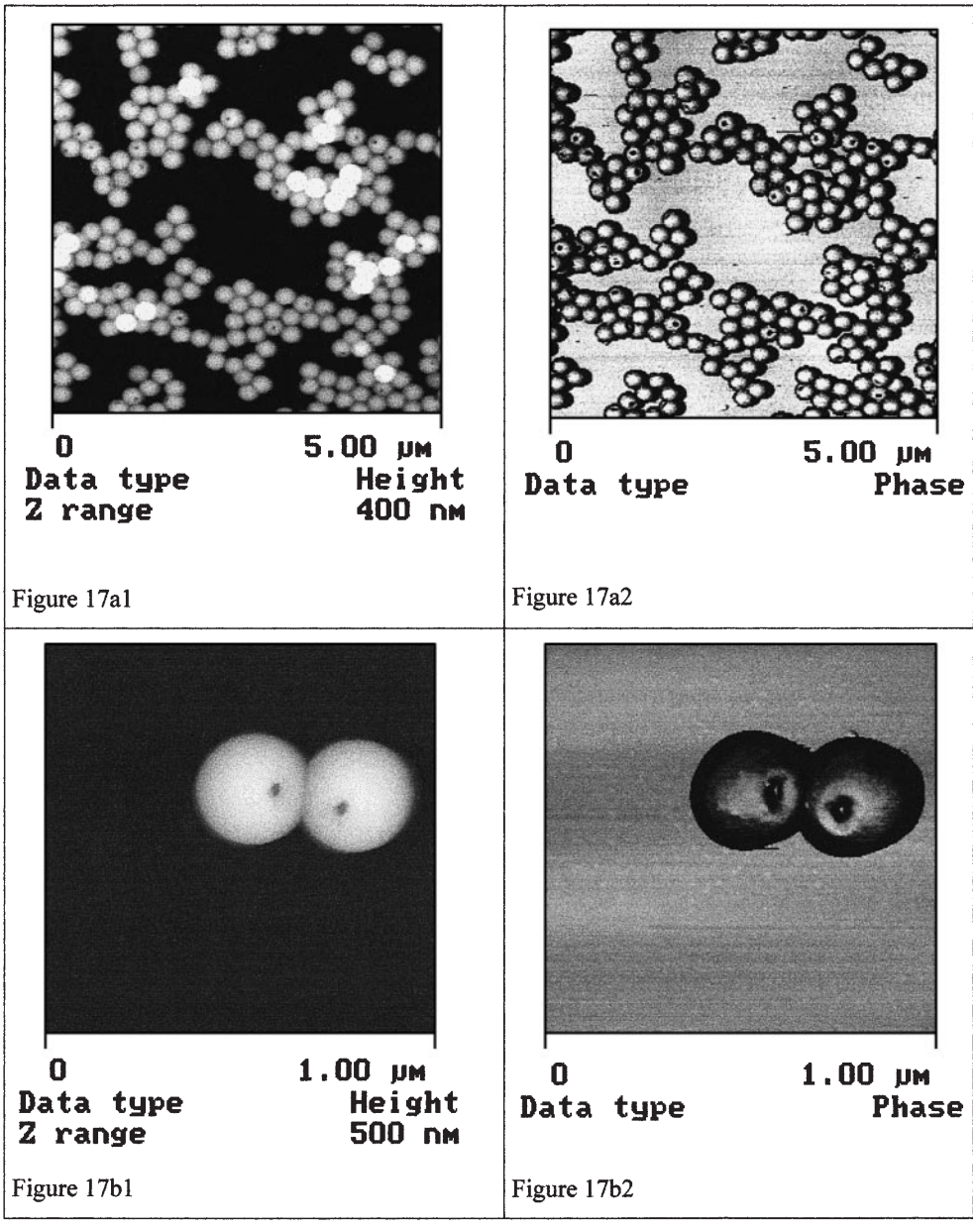

Fig. 17 a Atomic force measurement (*AFM*) pictures of the particles obtained with recipe C run D (sampling time 120 min); **a1** – height representation, **a2** – phase representation. **b** AFM picture of two anomalous particles obtained with recipe C run D (sampling time 120 min); **b1** – height representation, **b2** – phase representation

pictures in Fig. 17a and b should also represent the shape of anomalous particles in aqueous dispersions. Especially the magnification in Fig. 17b shows the hollows very clearly. Additionally, this scenario of the formation of anomalous structures is supported by the experimental fact that dispersions of lower-molecular-weight model oligomers st02 and st05 do not form anomalous particles upon swelling. These chains are so short that the particles may either reorganize completely, possibly after dissolution (st05), or even dissolve in the water-swelling-agent mixture (st02). Further support comes from the data depicted in Fig. 18 which clearly shows that the formation of indentations requires a medium-range molecular weight to ensure a balance between repulsion of hydrophilic head groups and hydrophobic attraction or entanglements between the chains. In the case of samples represented by curves 1 and 2 (recipes A and B) the average molecular weight as well as the monomer concentration inside the particles may be too low as swelling is restricted due to the particular experimental conditions. Curves 3 and 4 represent MWD of particles possessing anomalous morphologies. In contrast, particles with MWD represented by curve 5 do not have anomalous regions although the particles are highly swollen but the average molecular weight is obviously too high.

It is to be noted that also in surfactant-free emulsion polymerizations of styrene as well as of methyl methacrylate with PEGA initiators anomalous particle morphologies have been observed [2]. These initiators lead to particles consisting of block copolymers where phase separation, assuming chain mobility is high enough, takes place driven by the mutual incompatibility of the polymer blocks.

Finally, surfactant-free emulsion polymerization of hydrophobic monomers with hydrophilic initiators are nice examples of self-regulating systems with respect to colloidal stability. During the course of the polymerization the essential properties of the system (particle size, PSD, molecular weight, MWD, n_L, and particle morphology) develop in such a way that the free energy is minimized to ensure stability even over almost 1 year.

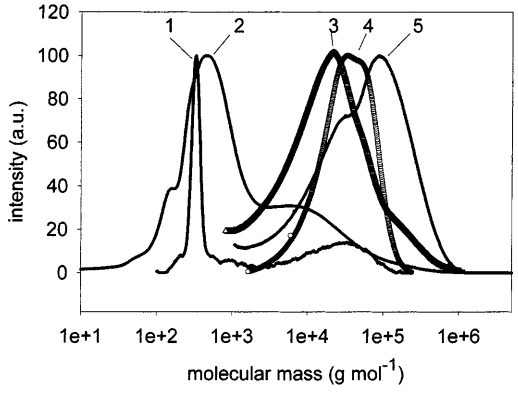

Fig. 18 Summary of molecular-weight distributions of samples prepared with different recipes. *1* – recipe A, no anomalous particles. *2* – recipe B no anomalous particles. *3* – recipe C, run C dialysed (sampling time 155 min), anomalous particles. *4* – recipe C, run D (sampling time 210 min), anomalous particles. *5* – recipe C, run A (sampling time 95 min), no anomalous particles

Acknowledgements The authors gratefully acknowledge the Max Planck Society for financial support, the receipt of a PhD fellowship for R.D. from BASF AG (Ludwigshafen, Germany), and the Max-Planck-Institute of Colloids and Interfaces for the possibility to use all the equipment needed. The authors are indebted to Rosemarie Rafler for carrying out a huge number of polymerizations, Sylvia Pirok and Brigitte Klein for an enormous number of analytical investigations, Gudrun Rother and Marlies Grävert for GPC measurements, Jürgen Hartmann and Rona Pitschke for all the TEM pictures, Hans-Peter Hentze for SEM pictures, Inga Stapff for AFM pictures, and Stephan Förster and Ines Below for preparing the model oligomers.

Appendix

For the thermal decomposition of persulfate Kolthoff and Miller [31] proposed the following mechanism:

$$S_2O_8^{2-} \xrightarrow{k_1} 2SO_4^{-}\cdot \tag{A1}$$

$$SO_4^{-}\cdot + H_2O \longrightarrow HSO_4^{-} + OH\cdot \tag{A2}$$

$$S_2O_8^{2-} + OH\cdot \longrightarrow HSO_4^{-} + SO_4^{-}\cdot + \frac{1}{2}O_2 \tag{A3}$$

$$OH\cdot + SO_4^{-}\cdot \longrightarrow HSO_4^{-} + \frac{1}{2}O_2 \tag{A4}$$

$$S_2O_8^{2-} + H_2O \longrightarrow 2HSO_4^{-} + \frac{1}{2}O_2 \tag{A5}$$

The decomposition rate simplifies to Eq. (A6) as reaction (A2) is the rate-determining step.

$$-\frac{d\left[S_2O_8^{2-}\right]}{dt} = k_1\left[S_2O_8^{2-}\right], \tag{A6}$$

where k_1 is the rate constant of reaction (A2), $\left[S_2O_8^{2-}\right]$ is the concentration of persulfate and t is the time. The rate constant k_1 at the temperature T is given by the Arrhenius equation [31] where R is the molar gas constant:

$$k_1(s^{-1}) = 1.23 \times 10^{17} \cdot \exp\left(-\frac{142.8(\text{kJ mol}^{-1})}{RT}\right). \tag{A7}$$

Integration of Eq. (A6) and solving for $\left[S_2O_8^{2-}\right]$ yields

$$\left[S_2O_8^{2-}\right] = \left[S_2O_8^{2-}\right]_0 \exp(-k_1 t). \tag{A8}$$

The same authors [31] proposed a hydrogen-ion catalysed decomposition of persulfate in acidic aqueous solution (without formation of new radicals):

$$S_2O_8^{2-} + H^+ \xrightarrow{k_2} HS_2O_8^- \quad \text{(A9)}$$

$$HS_2O_8^- \longrightarrow SO_4 + HSO_4^- \quad \text{(A10)}$$

$$SO_4 \longrightarrow SO_3 + \frac{1}{2}O_2 \quad \text{(A11)}$$

$$SO_3 + H_2O \longrightarrow H_2SO_4 \quad \text{(A12)}$$

$$H_2SO_4 \longrightarrow HSO_4^- + H^+ \quad \text{(A13)}$$

$$S_2O_8^{2-} + H_2O \xrightarrow{H^+} 2HSO_4^- + \frac{1}{2}O_2 \quad \text{(A14)}$$

If the uncatalysed and catalysed decompositions are considered to be independent reactions the rate of KPS decomposition is given by Eq. (A15) where k_2 is the rate constant of reaction (A9) with a temperature dependence given by Eq. (A16).

$$-\frac{d[S_2O_8^{2-}]}{dt} = k_1[S_2O_8^{2-}] + k_2[S_2O_8^{2-}][H^+], \quad \text{(A15)}$$

$$k_2(s^{-1}) = 36.25 \times 10^{13} \exp\left(-\frac{111.0(\text{kJ mol}^{-1})}{RT}\right) \quad \text{(A16)}$$

However, as hydrogen sulfate is produced according to both reaction schemes and its dissociation leads to a continuous increase in H^+ concentration both mechanisms are not independent. If the protolysis equilibrium is used to calculate the concentration of protons Eq. (A22) results according to Eq. (A17)–(A21) for the induced KPS decomposition where K_s is the acid constant of $[HSO_4^-]$. The index 0 denotes initial values.

$$K_s = \frac{[H^+][SO_4^{2-}]}{[HSO_4^-]} \quad \text{(A17)}$$

$$[HSO_4^-] = [HSO_4^-]_0 - [H^+], \quad [SO_4^{2-}] = [H^+] \quad \text{(A18)}$$

$$K_s = \frac{[H^+]^2}{[HSO_4^-]_0 - [H^+]} \quad \text{(A19)}$$

$$[H^+] = -\frac{K_s}{2} + \sqrt{\frac{K^2}{4} + K_s[HSO_4^-]_0} \quad \text{(A20)}$$

$$[HSO_4^-]_0 = 2\left([S_2O_8^{2-}]_0 - [S_2O_8^{2-}]\right) \quad \text{(A21)}$$

$$-\frac{d[S_2O_8^{2-}]}{dt} = k_1[S_2O_8^{2-}] + k_2[S_2O_8^{2-}] \times \left(-\frac{K_s}{2} + \sqrt{\frac{K_s^2}{4} + 2K_s\left([S_2O_8^{2-}]_0 - [S_2O_8^{2-}]\right)}\right) \quad \text{(A22)}$$

Equation (A22) can only be solved numerically; however, one can get an analytical solution if complete dissociation of hydrogen sulfate is assumed. Hydrogen sulfate is a strong acid with an acid constant of $pK_s = 1.92$ at 22 °C and hence, for an initiator concentration of $[S_2O_8^{2-}]_0 = 2.5$ mmole l^{-1} 76% of it is dissociated. Therefore, it is reasonable to assume complete dissociation at 60 °C so that Eq. (A23) becomes valid.

$$[H^+] = [HSO_4^-]_0 = 2\left([S_2O_8^{2-}]_0 - [S_2O_8^{2-}]\right) \quad \text{(A23)}$$

Then Eq. (A15) can be rewritten to get Eq. (A24) which leads after integration to Eq. (A25) where ϕ is given by Eq. (A26).

$$-\frac{d[S_2O_8^{2-}]}{dt} = k_1[S_2O_8^{2-}] + 2k_2[S_2O_8^{2-}] \times [S_2O_8^{2-}]_0 - 2k_2[S_2O_8^{2-}]^2 \quad \text{(A24)}$$

$$[S_2O_8^{2-}] = \frac{\phi[S_2O_8^{2-}]_0}{k_1 \exp(t\phi) + 2k_2[S_2O_8^{2-}]_0} \quad \text{(A25)}$$

$$\phi = k_1 + 2k_2[S_2O_8^{2-}]_0. \quad \text{(A26)}$$

As shown in Fig. A1 Eqs. (A22) and (A24) lead to identical results; however, the more important result for further calculations is the good agreement between curve 1 and curve 3 which shows that Eq. (A8) describes the KPS decomposition up to a time of almost 10 h pretty well.

As the polymerizations are carried out at a temperature of 60 °C molar conductivities at this temperature are needed for model calculations. For KPS and hydrogen sulfate values at 60 °C are not known. Conductivities at higher temperatures can be found only for some simple ions [54]. For protons, sulfate ions, and potassium ions the following equations were fitted from these data with ϑ as the temperature in degrees Celsius.

$$\Lambda_{H^+} = 226 + 5.06\vartheta - 2.4 \times 10^{-3}\vartheta^2 - 6.4 \times 10^{-5}\vartheta^3 \quad \text{(A27)}$$

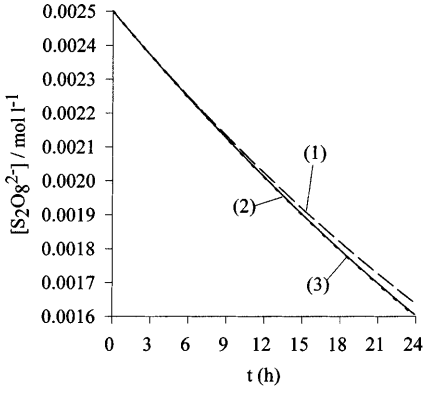

Fig. A1

$$\Lambda_{SO_4^{2-}} = 80 + 2.81\bar{3}\vartheta + 0.0128\vartheta^2 - 2.1\bar{3} \times 10^{-5}\vartheta^3 \quad \text{(A28)}$$

$$\Lambda_{K^+} = 38 + 1.37\bar{3}\vartheta + 3.6 \cdot 10^{-3}\vartheta^2 - 5.33 \times 10^{-6}\vartheta^3 \quad \text{(A29)}$$

As the ion mobility depends on the viscosity of water one can calculate $\Lambda_{S_2O_8^{2-}}$ and $\Lambda_{HSO_4^-}$, respectively, for different temperatures assuming a relationship described by Eq. (A30). For this reason Eq. (A31) fits the temperature dependence of the viscosity of water (η_w) in a temperature range between 20 and 100 °C [54].

$$\Lambda(T_2) = \Lambda(T_1)\frac{\eta_w(T_1)}{\eta_w(T_2)} \quad \text{(A30)}$$

$$\log\left(\frac{\eta_w(\vartheta)}{\eta_w(20\,^\circ\text{C})}\right) = \frac{1.3272(20-\vartheta) - 0.001053(\vartheta-20)^2}{\vartheta + 1.05}. \quad \text{(A31)}$$

Equivalent conductivities for all ions of interest for further consideration are summarized in Table 2. The values for persulfate ions and hydrogen sulfate ions calculated with Eqs. (A30) and (A31) integrate well into the values for the other ions calculated with Eqs. (A27)–(A29). So, a comparison between the values for all the ions listed in Table 2 proves the usefulness of this procedure.

Finally, Eq. (2) results from modelling the experimental conductivity behaviour during the initial stage of a KPS-initiated emulsion polymerization. For the calculations the following reasonable assumptions have been made $[K^+] = 2[S_2O_8^{2-}]_0 = \text{constant}$, $[S_2O_8^{2-}]$ from Eq. (A25), $[H^+]$ from Eq. (A23) and $[HSO_4^-] = [HSO_4^-]_0 - [H^+] = 0$. Furthermore, the KPS decomposition was calculated according to Eq. (A8) which is a good approximation as the polymerization time was always below 3 h.

References

1. Tauer K (1995) Polym Adv Technol 6: 435–440
2. Tauer K, Antonietti M, Rosengarten L, Müller H (1998) Macromol Chem Phys 199: 897–908
3. Kotera A, Furusawa K, Takeda Y (1970) Kolloid Z Z Polym 239: 677–681
4. Kotera A, Furusawa K, Kudo K (1970) Kolloid Z Z Polym 240: 837–841
5. Furusawa K, Norde W, Lyklema J (1972) Kolloid Z Z Polym 250: 908–909
6. Goodwin JW, Hearn J, Ho CC, Ottewill RH (1974) Colloid Polym Sci 252: 464–471
7. Goodwin JW, Hearn J, Ho CC, Ottewill RH (1973) Br Polym J 5: 347–362
8. Hearn J, Ottewill RH, Shaw JN (1970) Br Polym J 2: 116–120
9. Eshuis A, Leendertse HJ, Thoenes D (1991) Colloid Polym Sci 269: 1086–1089
10. Tuin G, Peters ACIA, van Diemen AJG Stein HN (1993) J Colloid Interface Sci 158: 508–510
11. Zhang W, Gao J, Wu C (1997) Macromolecules 30: 6388–6390
12. Tauer K, Neelsen J, Hellmich C (1985) Acta Polym 36: 665–670
13. Goodall AR, Wilkinson MC, Hearn J (1977) J Polym Sci Polym Chem Ed 15: 2193–2218
14. Goodall AR, Wilkinson MC, Hearn J (1980) In: Fitch RM (ed) Polymer Colloids II. Plenum, New York, pp 629–650
15. Kühn I, Tauer K (1995) Macromolecules 28: 8122–8128
16. Tauer K, I Kühn I (1997) In: Asua JM (ed) Polymeric dispersions: principles and applications. Kluwer, Dordrecht, pp 49–65
17. Cox RA, Creasey JM, Wilkinson MC (1974) Nature 252: 468–469
18. Goodall AR, Wilkinson MC, Hearn J (1975) J Colloid Interface Sci 53: 327–331
19. Cox RA, Wilkinson MC, Creasey J, Goodall AR, Hearn J (1977) J Polym Sci Polym Chem Ed 15: 2311–2319
20. Rupar W, Mitchell JM (1962) Rubber Chem Technol 35: 1028–1040
21. Feeney PJ, Napper DH, Gilbert RG (1987) Macromolecules 20: 2922–2930
22. Song Z, Poehlein GW (1989) J Colloid Interface Sci 128: 501–510
23. Rjabova MS, Sautin SN, Smirnov NI (1979) Zh Prikl Khim 52: 2065–2071
24. Chen S-A, Lee S-T (1992) Macromolecules 25: 1530–1533
25. Hearn J, Wilkinson MC, Goodall AR, Chainey M (1985) J Polym Sci Polym Chem Ed 23: 1869–1883
26. Chainey M, Hearn J, Wilkinson MC (1987) J Polym Sci Polym Chem Ed 25: 505–518
27. Chang H-S, Chen S-A (1987) Makromol Chem Rapid Commun 8: 297–304
28. Song Z, Poehlein GW (1990) J Polym Chem Polym Chem 28: 2359–2392
29. Tauer K, Deckwer R (1998) Acta Polym 49: 411–416
30. Tauer K, Müller H, Schellenberg C, Rosengarten L (1998) Colloids Surf A (in press)
31. Kolthoff IM, Miller IK (1951) J Am Chem Soc 73: 3055–3059
32. House DA (1962) Chem Rev 62: 185–203
33. Behrman EJ, Edwards JO (1980) Rev Inorg Chem 2: 179–206
34. Lane WH (1946) Ind Eng Chem Anal Ed 18: 295–296
35. Tauer K, Kühn I (1995) Macromolecules 28: 2236–2239
36. Ottewill RH, Shaw JN (1967) Kolloid Z Z Polym 218: 34–40
37. Smitham JB, Gibson DV, Napper DH (1973) J Colloid Interface Sci 45: 211–214
38. Stone-Masui J, Watillon A (1975) J Colloid Interface Sci 52: 479–503
39. Bagchi P, Gray BV, Birnbaum SM (1980) In: Fitch RM (ed) Polymer colloids II. Plenum, New York, pp 225–263
40. Stone-Masui JH, Stone WEE (1980) In: Fitch RM (ed) Polymer Colloids II. Plenum, New York, pp 331–360
41. Räder HJ, Schrepp W (1998) Acta Polym 49: 272–293
42. Buxton GV, Greenstock CL, Helman WP, Ross AB (1988) J Phys Chem Ref Data 17: 513–886
43. Jacobi B (1952) Angew Chem 18: 539–543

44. Ley G, Gerrens H (1971) Makromol Chem 175: 563–581
45. Gerrens H, Kuchner K, Ley G (1971) Chem Ing Tech 43: 693–740
46. Tauer K, Müller I (1993) Acta Polym 44: 285–293
47. Müller RH (ed) (1996) Zetapotential und Partikelladung in der Laborpraxis. Wissenschaftliche Verlagsgesellschaft, Stuttgart, pp 100–240
48. Bevington JC, Melville HW, Taylor RP (1954) J Polym Sci 12: 449–453
49. Bessiere J-M, Boutevin B, Loubet O (1993) Polym Bull 31: 673–677
50. Tauer K (1998) Macromolecules 31: 9390–9391
51. Moroi Y (1992) Micelles, theoretical and applied aspects. Plenum, New York, pp 16–18
52. Ohara PC, Leff DV, Heath JR, Gelbart WM (1995) Phys Rev Lett 75: 3466–3469
53. Förster S, Antonietti M (1998) Adv Mater 10: 195–217
54. Lide DR (ed) (1993) CRC Handbook of Chemistry and Physics. CRC Press, Boca Raton, pp 5-105–113